Showcasing research from Professor Zhaoyue Liu's laboratory, School of Chemistry, Beihang University, China.

Photosynthesis-inspired bifunctional energy-harvesting devices that convert light and salinity gradients into electricity

Inspired by the bifunctional utilization of light energy and a proton gradient in photosynthesis, we proposed conceptually an energy harvesting device that is capable of converting light and a salinity gradient into electricity simultaneously.

As featured in:

See Zhaoyue Liu *et al.*, *Chem. Commun.*, 2018, **54**, 12310.

ROYAL SOCIETY OF CHEMISTRY

rsc.li/chemcomm

Registered charity number: 207890

ChemComm

COMMUNICATION

View Article Online
View Journal | View Issue

Cite this: *Chem. Commun.*, 2018, **54**, 12310

Received 26th July 2018,
Accepted 17th September 2018

DOI: 10.1039/c8cc06076b

rsc.li/chemcomm

Photosynthesis-inspired bifunctional energy-harvesting devices that convert light and salinity gradients into electricity†

Huihui Ren,[a] Tianliang Xiao,[a] Qianqian Zhang[b] and Zhaoyue Liu *[a]

Inspired by the bifunctional utilization of light energy and a proton gradient in photosynthesis, we proposed conceptually an energy-harvesting device that is capable of converting light and a salinity gradient into electricity simultaneously. Our bioinspired concept provided a potential opportunity to harvest multiple renewable energies and maximize the overall power output.

The conversion of renewable energy into electrical energy is considered to possibly help solve the future energy crisis.[1,2] Light and salinity gradients are two kinds of clean and abundant renewable energy that exist ubiquitously on our earth.[3–7] Generally, light energy can be converted into electricity by a photoelectric effect that a photon creates on an electron–hole pair in a semiconductor electrode, and subsequently the light-induced electron transfers to the external load.[8,9] Correspondingly, the salinity gradient can be converted into electrical energy *via* reverse electrodialysis based on an ion-selective membrane, which recently received significant attention for the utilization of abundant "blue" energy in the ocean.[10–18] However, the present energy conversion device can harvest only one kind of renewable energy, which restricts its overall power output. The integration of different energy conversion processes into a single energy conversion device is considered to be able to maximize its overall power output.[19] Therefore, the realization of simultaneous conversion of light and a salinity gradient into electricity provides an opportunity to potentially improve the overall power output of the energy-conversion device.

Photosynthesis is one of the most important biological processes that achieves energy flow and matter cycling in nature.[20–23] In green plants, photosynthesis occurs in the chloroplasts, and initiates from the excitation of chlorophyll molecules in the thylakoid membrane by sunlight. The light-induced holes transfer to the oxygen-evolving complexes for the oxidation of water molecules into oxygen and protons, which converts light energy into chemical energy (Scheme 1A).[24,25] Simultaneously, the light-induced electrons transfer to nicotinamide adenine dinucleotide phosphate hydrogen (NADPH), which creates a proton gradient across the thylakoid membrane. The proton gradient is eventually converted into chemical energy through the formation of adenosine triphosphate (ATP) from adenosine triphosphate (ADP) (Scheme 1A).[26–29] This bifunctional utilization of light energy and proton gradients for energy flow in photosynthesis inspired us to develop a new type of energy-conversion device.

Herein, inspired by the photosynthesis in green plants, we propose conceptually a bifunctional energy-harvesting device that is capable of converting light and a salinity gradient into electricity simultaneously. As shown in Scheme 1B, our proof-of-concept device comprised a custom-built two-chamber electrochemical cell, which was divided into two regions: an

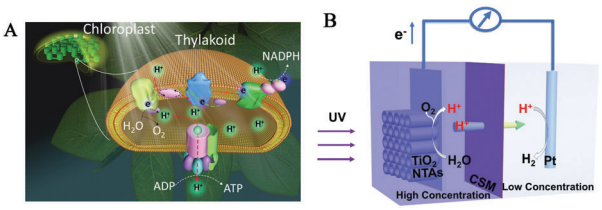

Scheme 1 (A) Bifunctional utilization of light energy and a proton gradient for energy flow in the photosynthesis of green plants. The light energy is converted into chemical energy through the oxidization of water molecules into oxygen and protons by the light-induced holes in the excited chlorophyll molecules. Simultaneously, the proton gradient across the thylakoid membrane is converted into chemical energy stored in adenosine triphosphate (ATP). (B) Schematic diagram for the photosynthesis-inspired bifunctional energy-harvesting device. A TiO_2 electrode consisting of nanotubular arrays (NTAs) was used as a model anode to harvest the light energy. A chemically inert Pt electrode was used as a cathode to relay the light-induced electrons from the TiO_2 electrode. The salinity gradient was introduced from the anode to the cathode using Na_2SO_4 aqueous electrolytes with different concentrations, which were separated by a cation-selective membrane (CSM).

[a] *Key Laboratory of Bio-Inspired Smart Interfacial Science and Technology of Ministry of Education, School of Chemistry, Beihang University, Beijing 100191, P. R. China. E-mail: liuzy@buaa.edu.cn; Tel: +86-10-82317801*

[b] *The College of Materials Science and Engineering, Beijing University of Technology, Beijing 100124, P. R. China*

† Electronic supplementary information (ESI) available: Experimental details, and SEM images. See DOI: 10.1039/c8cc06076b

anode and a cathode. The anode and cathode regions were filled with Na_2SO_4 aqueous electrolytes with a high and low concentration respectively, which were separated by a cation-selective membrane. A TiO_2 electrode consisting of nanotubular arrays (NTAs)[30–32] was used as a model anode to harvest the light energy (herein, the light energy was from UV light). A chemically inert Pt electrode was used as a cathode to relay the light-induced electrons from the TiO_2 electrode. Under UV irradiance, the light-induced electrons in the TiO_2 electrode transferred to an external circuit, which achieved the conversion of light energy into electricity. The salinity gradient across the anode and the cathode enhanced the power output of the device under UV illumination, which verified the conversion of the salinity gradient into electrical energy. Our bioinspired concept provided a potential opportunity to harvest multiple renewable energies and maximize the overall power output of an energy-conversion device.

It has been well-recognized that TiO_2 NTAs provide an intuitive one-dimensional electric pathway, which overcomes the boundary effect in the conventional TiO_2 mesoporous layer of nanoparticles and demonstrates significant potential applications in photoelectric conversion.[33–35] The typical top-viewed and cross-sectional SEM images of TiO_2 NTAs are shown in Fig. S1, ESI.† After anodization, large-scale, uniform and well-defined TiO_2 NTAs were grown on the surface of the Ti substrate (Fig. S1A, ESI†). The average internal diameter of the NTAs was determined to be ~72.5 nm and the wall thickness was ~14.9 nm (Fig. S1B, ESI†). The cross-sectional image of Fig. S1C (ESI†) indicates that TiO_2 NTAs with a length of ~251 nm were vertical to the Ti substrate. The short length of the TiO_2 NTAs reduced the transport distance of light-induced electrons to the Ti substrate, which was favorable for the generation of a photocurrent. The XRD results indicated that the TiO_2 NTAs demonstrated anatase crystallization, as evidenced by the characteristic diffraction peak at $2\theta = 25.0^\circ$ (Fig. S1D, ESI†).

First, we investigated the photoelectric conversion behavior of TiO_2 NTAs in a two-electrode configuration without a salinity gradient. In this case, the anode and cathode regions of the device were filled with Na_2SO_4 solutions with the same concentrations ($c_{Na_2SO_4}$), which were separated by a cation-selective membrane. As shown by the *I–V* curves in Fig. 1A, under 5.7 mW cm^{-2} UV illumination, the device outputted a stable light-induced short-circuit current (I_{sc}) and open-circuit voltage (V_{oc}), indicating that the light energy was converted into electricity. Following the increase in $c_{Na_2SO_4}$ from 1 mM to 100 mM, the outputted I_{sc} increased from 6.52 to 12.82 μA cm^{-2} as a result of the enhanced ion conductivity (Fig. 1B). The outputted maximal power density (P_{max}) increased from 0.58 μW cm^{-2} to 0.98 μW cm^{-2} (Fig. 1C). Correspondingly, the outputted V_{oc} increased slightly from 0.71 to 0.73 V (Fig. 1A), showing a small dependence on the concentration of $c_{Na_2SO_4}$ because the V_{oc} was mainly determined by the Fermi level of TiO_2 under UV illumination. Note that a further increase of $c_{Na_2SO_4}$ to 1 M did not contribute to an improvement of I_{sc} and P_{max} (Fig. 1B and C), which implied that the ion conductivity of Na_2SO_4 solution with a concentration of 100 mM–1 M was enough to maximize the light-induced current output. Fig. 1D shows that

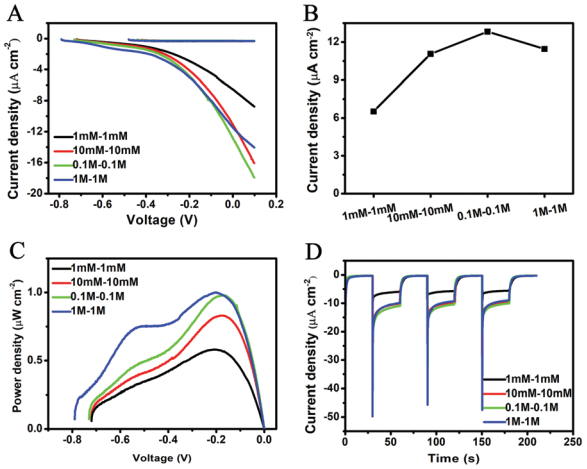

Fig. 1 (A) Current–voltage (*I–V*) curves of TiO_2 NTAs in a two-electrode configuration without a salinity gradient. The anode and cathode regions of the device were filled with Na_2SO_4 solutions with the same concentrations (1 mM, 10 mM, 0.1 M and 1 M), which were separated by a cation-selective membrane. (B) Relation between the short-circuit current density (I_{sc}) of TiO_2 NTAs and the concentrations of Na_2SO_4 solution. (C) Power output of TiO_2 NTAs in Na_2SO_4 solution with different concentrations. (D) Evolution of the I_{sc} when the UV irradiance was switched on and off alternately. The generation of I_{sc} was completely ascribed to the harvesting of the light energy.

the light-induced I_{sc} of our device decreased to zero when the UV irradiance was switched off. As soon as the irradiance was switched on again, the I_{sc} almost recovered to its original value, which indicated that the outputted I_{sc} was completely ascribed to the harvesting of the light energy. The conversion of light energy into electricity by TiO_2 NTAs is considered to be achieved by the light-induced redox reaction on the anode and the cathode.[8] Following the excitation of the TiO_2 anode by UV illumination, the light-induced holes on the valence band of TiO_2 oxidize the water molecules to generate protons. Simultaneously, the light-induced electrons on the conduction band of TiO_2 transfer to the Pt cathode through an external circuit. At the cathode, the light-induced electrons are consumed by the reduction of the protons that transported from the anode across the cation-selective membrane (Scheme 1B). The overall reaction of light-induced water decomposition contributes to the conversion of light energy into electricity.

Then, we introduced a salinity gradient from the anode to the cathode in our device to enhance the current output under UV illumination. The concentrations of the Na_2SO_4 solutions in the anode (TiO_2) and cathode (Pt) region were denoted as c_A and c_c respectively. As shown in Fig. 2(A1–A3), at $c_A = c_c = 0.1$ M and 1 M, the device outputted an I_{sc} of 12.82 and 11.45 μA cm^{-2} respectively under 5.7 mW cm^{-2} UV illumination. When a 10-fold salinity gradient of c_A/c_c = 1 M/0.1 M was introduced, an I_{sc} of 16.34 μA cm^{-2} was generated, which was enhanced by ~27.5% when compared with that at $c_A = c_c = 0.1$ M (12.82 μA cm^{-2}). The outputted V_{oc} was enhanced slightly from 0.73 V at $c_A = c_c = 0.1$ M to 0.80 V at c_A/c_c = 1 M/0.1 M because of the potential difference across the cation-selective membrane formed by the salinity gradient. Correspondingly, the outputted P_{max} increased from

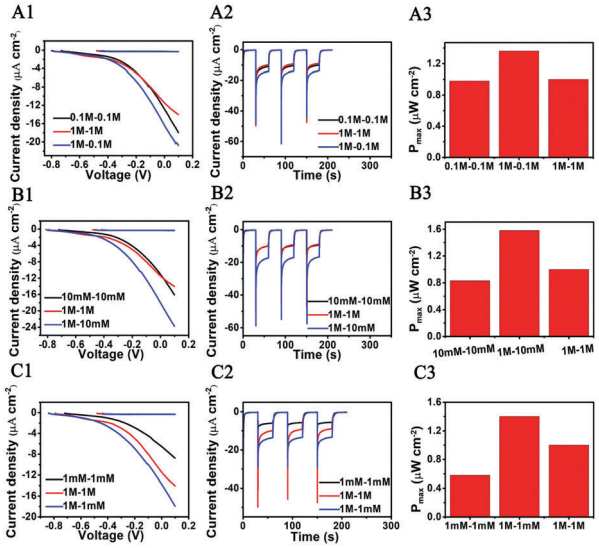

Fig. 2 Current–voltage (I–V) curves, short-circuit current–time (I_{sc}–t) curves and maximal power output (P_{max}) of the energy conversion device under UV illumination with and without a salinity gradient. (A1–A3) A 10-fold salinity gradient of c_A/c_c = 1 M/0.1 M. (B1–B3) A 100-fold salinity gradient of c_A/c_c = 1 M/10 mM. (C1–C3) A 1000-fold salinity gradient of c_A/c_c = 1 M/1 mM. The concentrations of Na_2SO_4 solution in anode (TiO_2) and cathode (Pt) regions were denoted as c_A and c_c respectively. For a clear comparison, the performances of the device at the corresponding Na_2SO_4 concentration without a salinity gradient ($c_A = c_c$) are also shown. A salinity gradient enhanced the outputted I_{sc}, V_{oc} and P_{max} of the device under UV illumination, which demonstrated that the light energy and salinity gradient were converted into electricity simultaneously.

0.98 to 1.36 μW cm^{-2} by 38.8%. When the salinity gradient increased 100-fold at c_A/c_c = 1 M/0.01 M, the device generated an I_{sc} of 18.00 μA cm^{-2}, which was improved by ~57.2% when compared with that (11.45 μA cm^{-2}) at $c_A = c_c$ = 1 M. The outputted V_{oc} increased from 0.79 V at $c_A = c_c$ = 1 M to 0.81 V at c_A/c_c = 1 M/0.01 M (Fig. 2B1–B3). Correspondingly, the outputted P_{max} increased from 1.00 to 1.58 μW cm^{-2} by 58%. When a 1000-fold gradient at c_A/c_c = 1 M/0.001 M was introduced into the device, the outputted I_{sc} of 13.76 μA cm^{-2} was also enhanced obviously when compared with that at $c_A = c_c$ = 1 M (Fig. 2C1–C3). However the enhanced percentage of the outputted P_{max} was only ~40%, which was much lower than that at a 100-fold salinity gradient. This was explained by the fact that the low ion conductivity of 1 mM Na_2SO_4 solution suppressed the current generation from the salinity gradient. Correspondingly, the outputted V_{oc} was enhanced from 0.79 V at $c_A = c_c$ = 1 M to 0.84 V at c_A/c_c = 1 M/0.001 M resulting from a high potential difference across the cation-selective membrane at a high salinity gradient. When the UV irradiance was switched off, the light-induced I_{sc} of our device under the salinity gradient decreased to zero as shown in Fig. 2A2, B2 and C2. This was explained by the fact that the conversion of the salinity gradient into electrical energy was achieved by the light-induced redox reaction on the anode and the cathode. Therefore, the synergistic effect between the light and the salinity gradient was essentially important for converting the salinity gradient into electricity. The above results indicated clearly that a salinity gradient enhanced the outputted I_{sc} and P_{max} of our device under UV illumination, which demonstrated that the light energy and the salinity gradient energy were converted into electricity simultaneously.

The mechanism for the conversion of light energy and the salinity gradient into electric energy is shown in Fig. 3A and B. Under UV illumination, a light-induced potential difference (E_L) was formed between the TiO_2 anode (negative electrode) and the Pt cathode (positive electrode), which was determined by the Fermi level of TiO_2 and the redox potential of the Pt electrode. The light-generated protons formed on the TiO_2 anode needed to transport through the cation-selective membrane to the Pt cathode, on which the protons were reduced by the light-induced electrons from the anode (Fig. 3A). Therefore, a fast diffusion of protons to the cathode would reduce the recombination between the light-induced electrons and protons on the anode, which was essentially important for the conversion of light energy into electricity. When a salinity gradient was introduced from the anode to the cathode separated by a cation-selective membrane, the Na^+ ions diffuse preferentially from the high to low concentration, which forms a diffusion potential (E_{diff}) across the membrane.[36,37] The same polarity of E_{diff} with that of E_L accelerated the diffusion of protons from the anode to the cathode, which reduced the charge recombination between the light-induced electrons and protons on the anode and enhanced the generation of current (Fig. 3B). Moreover, following the increase of c_A/c_c from 10 to 100, the increased value of E_{diff} resulted in more effective generation of current.

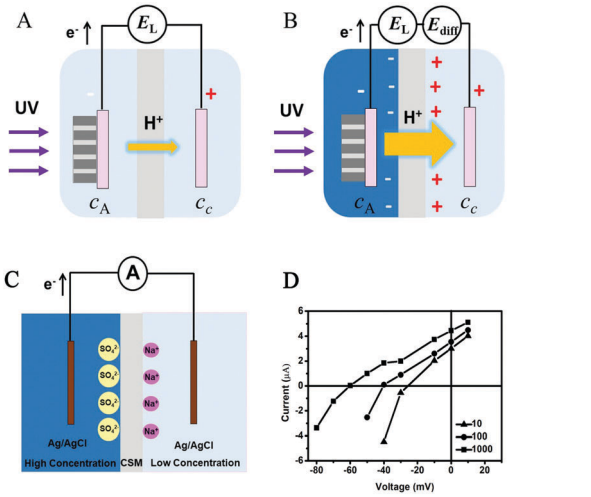

Fig. 3 (A and B) Schematic mechanism for the generation of electricity from the energy conversion device under UV illumination without (A) and with (B) a salinity gradient. The UV illumination generated a light-induced potential difference (E_L) between the TiO_2 anode (negative) and the Pt cathode (positive). The salinity gradient from the anode to the cathode formed a diffusion potential (E_{diff}) across the membrane. The same polarity of E_{diff} with that of E_L accelerated the diffusion of protons from the anode to the cathode, which reduced the charge recombination between the light-induced electrons and protons on the anode and enhanced the generation of current. (C) Schematic diagram for the measurement of diffusion potential (E_{diff}). (D) Current–voltage (I–V) curves of the cation-selective membrane under different salinity gradients of c_A/c_c = 10, 100 and 1000. The E_{diff} across the membrane was read from the intercept of the I–V curve on the voltage axis (V_{oc}).

The diffusion potential (E_{diff}) across the cation-selective membrane formed by the salinity gradient could be determined from the *I–V* curve of the cation-selective membrane. The schematic setup for the measurements is shown in Fig. 3C. The measured potential difference between the two Ag/AgCl electrodes (E_{mea}) included two contributions from the redox potential difference (E_{redox}) of the two Ag/AgCl electrodes and the E_{diff} across the cation-selective membrane.[13,18,36] The E_{redox} was ignored because the potential of the Ag/AgCl electrode was only dependent on the concentration of Cl^- ions. Therefore, the E_{mea} was approximately equal to the E_{diff}, which was read from the intercept of the *I–V* curve on the voltage axis. The *I–V* curves of the cation-selective membrane under different salinity gradients of c_A/c_c are shown in Fig. 3D. It was demonstrated that the values of E_{diff} increased following the increase of the salinity gradient of c_A/c_c. When the salinity gradient was 10-, 100- and 1000-fold, the E_{diff} read from the intercept of the *I–V* curve on the voltage axis was 22.9, 40.3 and 60.3 mV. Our results certified that the existence of a diffusion potential across the membrane contributed to the enhancement of the overall power output of the device under illumination.

In summary, we proposed conceptually a photosynthesis-inspired bifunctional energy-harvesting device that converted light energy and a salinity gradient into electricity simultaneously. In the proof-of-concept device, the light-active TiO_2 anode consisting of nanotubular array electrodes achieved the conversion of light energy into electricity based on the light-induced charge separation under UV illumination. A salinity gradient from the anode to the cathode impressively improved the overall power output of the device by 58%, which verified the effective conversion of the salinity gradient into electricity. Our bioinspired concept provided a potential opportunity to harvest multiple renewable energies and maximized the overall power output of an energy-conversion device.

This work was supported by the National Key Research and development Program of China (2017YFA0206902 and 2017YFA0206900), the National Natural Science Foundation of China (21571011 and 21701003), the National Basic Research Program of China (2014CB931803), the China Postdoctoral Science Foundation (Grant no. 2015M580035 and 2017T100022) and the Fundamental Research Funds for the Central Universities (YWF-18-BJ-J-71).

Conflicts of interest

There are no conflicts to declare.

Notes and references

1 S. Chu and A. Majumdar, *Nature*, 2012, **488**, 294–303.
2 J. C. Crittenden and H. S. White, *J. Am. Chem. Soc.*, 2010, **132**, 4503–4505.
3 M. Grätzel, *Nature*, 2001, **414**, 338–344.
4 A. Hagfeldt, G. Boschloo, L. Sun, L. Kloo and H. Pettersson, *Chem. Rev.*, 2010, **110**, 6595–6663.
5 N. S. Lewis, *Science*, 2016, **351**, aad1920.
6 B. E. Logan and M. Elimelech, *Nature*, 2012, **488**, 313–319.
7 J. Feng, M. Graf, K. Liu, D. Ovchinnikov, D. Dumcenco, M. Heiranian, V. Nandigana, N. R. Aluru, A. Kis and A. Radenovic, *Nature*, 2016, **536**, 197–200.
8 A. Fujishima and K. Honda, *Nature*, 1972, **238**, 37–38.
9 B. O'Regan and M. Grätzel, *Nature*, 1991, **353**, 737–740.
10 N. Y. Yip, D. Brogioli, H. V. M. Hamelers and K. Nijmeijer, *Environ. Sci. Technol.*, 2016, **50**, 12072–12094.
11 N. Y. Yip and M. Elimelech, *Environ. Sci. Technol.*, 2012, **46**, 5230–5239.
12 W. Guo, L. Cao, J. Xia, F. Nie, W. Ma, J. Xue, Y. Song, D. Zhu, Y. Wang and L. Jiang, *Adv. Funct. Mater.*, 2010, **20**, 1339–1344.
13 J. Gao, W. Guo, D. Feng, H. Wang, D. Zhao and L. Jiang, *J. Am. Chem. Soc.*, 2014, **136**, 12265–12272.
14 Z. Zhang, X. Kong, K. Xiao, Q. Liu, G. Xie, P. Li, J. Ma, Y. Tian, L. Wen and L. Jiang, *J. Am. Chem. Soc.*, 2015, **137**, 14765–14772.
15 L. Zhang and X. Chen, *Angew. Chem., Int. Ed.*, 2013, **52**, 7640–7641.
16 G. Z. Ramon, B. J. Feinberg and E. M. V. Hoek, *Energy Environ. Sci.*, 2011, **4**, 4423–4434.
17 S. Tseng, Y. Li, C. Lin and J. Hsu, *Nanoscale*, 2016, **8**, 2350–2357.
18 H. Chang, E. Choi and J. Park, *Lab Chip*, 2016, **16**, 700–708.
19 J. Duan, T. Hu, Y. Zhao, B. He and Q. Tang, *Angew. Chem., Int. Ed.*, 2018, **57**, 5746–5749.
20 D. Gust, T. A. Moore and A. L. Moore, *Acc. Chem. Res.*, 2001, **34**, 40–48.
21 J. H. Kim, M. Lee, J. S. Lee and C. B. Park, *Angew. Chem., Int. Ed.*, 2012, **51**, 517–520.
22 Q. Zhang, T. Xiao, N. Yan, Z. Liu, J. Zhai and X. Diao, *Nano Energy*, 2016, **28**, 188–194.
23 K. Tang, L. Zhu, V. S. Urban, A. M. Collins, P. Biswas and R. E. Blankenship, *Langmuir*, 2011, **27**, 4816–4828.
24 J. Barber, *Chem. Soc. Rev.*, 2009, **38**, 185–196.
25 D. Gust, T. A. Moore and A. L. Moore, *Acc. Chem. Res.*, 2009, **42**, 1890–1898.
26 J. Rochaix, *Science*, 2013, **342**, 50–51.
27 W. White, C. D. Sanborn, R. S. Reiter, D. M. Fabian and S. Ardo, *J. Am. Chem. Soc.*, 2017, **139**, 11726–11733.
28 X. Xie, G. A. Crespo, G. Mistlberger and E. Bakker, *Nat. Chem.*, 2014, **6**, 202–207.
29 X. Xie and E. Bakker, *Phys. Chem. Chem. Phys.*, 2014, **16**, 19781–19789.
30 Q. Cai, M. Paulose, O. K. Varghese and C. A. Grimes, *J. Mater. Res.*, 2005, **20**, 230–236.
31 K. Lee, A. Mazare and P. Schmuki, *Chem. Rev.*, 2014, **114**, 9385–9454.
32 Z. Liu, V. Subramania and M. Misra, *J. Phys. Chem. C*, 2009, **113**, 14028–14033.
33 K. Zhu, N. R. Neale, A. Miedaner and A. J. Frank, *Nano Lett.*, 2007, **7**, 69–74.
34 J. R. Jennings, A. Ghicov, L. M. Peter, P. Schmuki and A. B. Walker, *J. Am. Chem. Soc.*, 2008, **130**, 13364–13372.
35 G. K. Mor, K. Shankar, M. Paulose, O. K. Varghese and C. A. Grimes, *Nano Lett.*, 2006, **6**, 215–218.
36 D. Kim, C. Duan, Y. Chen and A. Majumdar, *Microfluid. Nanofluid.*, 2010, **9**, 1215–1224.
37 M. Nishizawa, V. P. Menon and C. R. Martin, *Science*, 1995, **268**, 700–702.